Structural Characterization and Magnetic Properties of the First 2,2′-Bipyrimidine-Containing Iron(III) Complexes

Giovanni De Munno,*[1a] Walter Ventura,[1a] Guillaume Viau,[1b,c] Francesc Lloret,[1b] Juan Faus,[1b] and Miguel Julve*[1b]

Dipartimento di Chimica, Università degli Studi della Calabria, 87030 Arcavacata di Rende, Cosenza, Italy, and Departament de Química Inorgànica, Facultat de Química de la Universitat de València, Dr. Moliner 50, 46100 Burjassot, València, Spain

Received August 29, 1997

Two new iron(III) complexes of the formulas $[Fe(bpm)Cl_3(H_2O)]\cdot H_2O$ (**1**) and $[Fe_2(bpm)Cl_6(H_2O)_2]\cdot 2H_2O$ (**2**) (bpm = 2,2′-bipyrimidine) have been synthesized and their crystal structures determined by single-crystal X-ray diffraction. **1** and **2** crystallize in the monoclinic system, space group $P2_1/n$, with $a = 8.593(2)$ Å, $b = 17.669(4)$ Å, $c = 8.928(2)$ Å, $\beta = 102.36(2)°$, and $Z = 4$ for **1** and $a = 6.422(3)$ Å, $b = 11.999(4)$ Å, $c = 12.297(6)$ Å, $\beta = 93.82(4)°$, and $Z = 2$ for **2**. The structure of complex **1** is made up of neutral $[Fe(bpm)Cl_3(H_2O)]$ mononuclear units and water molecules of crystallization. The monuclear units are linked through hydrogen bonds involving the coordinated water molecule and one of the chlorine atoms yielding a uniform chain. The iron(III) is hexacoordinate, with two nitrogens of a chelating bpm, three chlorine atoms, and one water molecule building a distorted octahedron around the metal atom. The structure of **2** consists of centrosymmetric bpm-bridged dinuclear $[Fe_2(bpm)(Cl_6)(H_2O)_2]$ units and water molecules of crystallization which are linked through hydrogen bonds leading to a three-dimensional network. The geometry of each metal atom in **2** is distorted octahedral as in **1**. The equatorial positions around the metal ion in **1** and **2** are filled by two bpm nitrogens and two chlorine atoms, whereas the axial positions are occupied by a water molecule and a chlorine atom. The shortest intermolecular metal−metal distance in **1** is 5.957(2) Å, and the intramolecular metal−metal separation in **2** is 5.952(1). The magnetic behavior of **1** and **2** has been investigated over the temperature range 1.8−300 K. Significant antiferromagnetic coupling is observed for both compounds, the susceptibility curves exhibiting maxima at 5.0 (**1**) and 5.2 K (**2**). The pathways of the exchange interaction in **1** (hydrogen bonding) and **2** (hydrogen bonding and bridging bpm) are discussed in the light of their crystal structures, and the values of the coupling constants are compared with those of related systems.

Introduction

During the past decade, we have undertaken a systematic study investigation of the complex formation between 2,2′-bipyrimidine (bpm) and the divalent first-row transition-metal ions.[2,3] The main goals in this field are the rational preparation of polynuclear compounds of controlled nuclearity with novel and interesting magnetic properties. The chelating and bis-chelating coordination modes of bpm make easy the preparation of mono- and dinuclear bpm-containing compounds, which can be used as precursors of higher-nuclearity systems. The synthetic strategy consisting of using these mono- and dinuclear species as complex ligands allowed us to establish preparative routes of two families of new magnetic materials: (i) homometallic chains which exhibit a regular alternation of ferro- and antiferromagnetic interactions, with the local spins ranging from $^1/_2$ to $^5/_2$;[4,5] and (ii) honeycomb layered materials with alternating antiferro- (through bpm and oxalate bridges)[6] or antiferro- (through bpm) and ferromagnetic (through double end-on azido bridges).[7] A very rare situation has been found in the case of Mn(II) where two compounds with the same formula, $[Mn_2(bpm)(N_3)_4]$, were obtained:[7a] one is bidimensional, and the other is tridimensional, the magnetic behavior being overall ferromagnetic for the former and antiferromagnetic for the latter.

In our attempts to extend these studies to trivalent first-row transition-metal ions, the first bpm-containing iron(III) complexes of the formulas $[Fe(bpm)Cl_3(H_2O)]\cdot H_2O$ (**1**) and $[Fe_2(bpm)Cl_6(H_2O)_2]\cdot 2H_2O$ (**2**) were obtained. Their crystal structures and magnetic properties are the subject of the present work.

Experimental Section

Materials. Iron(III) chloride and 2,2′-bipyrimidine were purchased from commercial sources and used as received; elemental analysis (C,

(1) (a) Università degli Studi della Calabria. (b) Universitat de València. (c) Permanent address: Laboratoire de Chimie des Matériaux Divisés et Catalyse, Université Paris 7, Denis Diderot, Paris (France).

(2) De Munno, G.; Julve, M. In *Metal Ligand Interactions. Structure and Reactivity*; Russo, N., Salahub, D. R., Eds.; NATO ASI Series 474; Kluwer: Dordrecht, 1996; p 139.

(3) De Munno, G.; Lloret, F.; Julve, M. In *Magnetism: A Supramolecular Function*; Kahn, O., Ed.; NATO ASI Series 484; Kluwer: Dordrecht, 1996; p 555.

(4) (a) De Munno, G.; Julve, M.; Lloret, F.; Faus, J.; Verdaguer, M.; Caneschi, A. *Angew. Chem., Int. Ed. Engl.* **1993**, *32*, 1046; (b) *Inorg. Chem.* **1995**, *34*, 157.

(5) (a) Viau, G.; Lombardi, M. G.; De Munno, G.; Julve, M.; Lloret, F.; Faus, J.; Caneschi, A.; Clemente-Juan, J. M. *Chem. Commun.* **1997**, 1195. (b) Cortés, R.; Drillon, M.; Solans, X.; Lezama, L.; Rojo, T. *Inorg. Chem.* **1997**, *36*, 677.

(6) De Munno, G.; Ruiz, R.; Lloret, F.; Faus, J.; Sessoli, R.; Julve, M. *Inorg. Chem.* **1995**, *34*, 408.

(7) (a) De Munno, G.; Julve, M.; Viau, G.; Lloret, F.; Faus, J.; Viterbo, D. *Angew. Chem., Int. Ed. Engl.* **1996**, *35*, 1807. (b) Cortés, R.; Lezama, L.; Pizarro, J. L.; Arriortua, M. I.; Rojo, T. *Angew. Chem., Int. Ed. Engl.* **1996**, *35*, 1810.

S0020-1669(97)01110-5 CCC: $15.00
Published on Web 03/12/1998

Table 1. Crystallographic Data[a] for $[Fe(bpm)Cl_3(H_2O)]\cdot H_2O$ (**1**) and $[Fe_2(bpm)Cl_6(H_2O)_2]\cdot 2H_2O$ (**2**)

compd	**1**	**2**
formula	$C_8H_{10}Cl_3FeN_4O_2$	$C_8H_{14}Cl_6Fe_2N_4O_4$
fw	356.4	554.6
space group	$P2_1/n$	$P2_1/n$
a, Å	8.593(2)	6.422(3)
b, Å	17.669(4)	11.999(4)
c, Å	8.928(2)	12.297(6)
β, deg	102.36	93.82(4)
V, Å^3	1324.1(5)	945.5(7)
Z	4	2
λ, Å	0.710 73	0.710 73
ρ_{calcd}, g cm^{-3}	1.788	1.948
T, °C	25	25
μ(Mo Kα), cm^{-1}	17.4	24.0
R^a	0.035	0.026
$R_w{}^b$	0.039	0.029

[a] $R = \sum(||F_o| - |F_c||)/\sum|F_o|$. [b] $R_w = [\sum w(|F_o| - |F_c|)^2/\sum w|F_o|^2]^{1/2}$.

H, N) was performed by the Microanalytical Service of the Università degli Studi della Calabria (Italy).

Synthesis. Compounds **1** and **2** were obtained as irregular yellow-orange (**1**) or irregular orange crystals (**2**) from orange aqueous solutions containing stoichiometric amounts of $FeCl_3$ (0.2 mmol) and bpm [0.2 (**1**) or 0.1 (**2**) mmol] by slow evaporation at room temperature. Both compounds are very soluble in water, and crystals appeared after the solutions were reduced nearly to dryness. The solid products were filtered off and washed with small amounts of ethanol and diethyl ether. Anal. Calcd for $C_8H_{10}Cl_3FeN_4O_2$ (**1**): C, 26.96; H, 2.83; N, 15.72. Found: C, 26.54; H, 2.64; N, 15.59. Anal. Calcd for $C_8H_{14}Cl_6Fe_2N_4O_4$ (**2**): C, 17.32; H, 2.54; N, 10.10. Found: C, 17.14; H, 2.42; N, 9.95.

The coexistence of uncoordinated and coordinated water molecules in **1** and **2** is consistent with the occurrence of a broad feature centered at about 3300 cm^{-1} (antisymmetric and symmetric OH stretching) and medium-intensity peaks at 1640 cm^{-1} (HOH bending) and 690 and 660 cm^{-1} (rocking and wagging frequencies of coordinated water).[8] The most significant difference between the infrared spectrum of **1** and that of **2** concerns the ring-stretching modes of bpm, which appears as a doublet of two intense and sharp bands at 1575 and 1560 cm^{-1} in the former and an intense and sharp peak at 1580 cm^{-1} with a weak absorption at 1565 cm^{-1} in the latter compound. This pattern is characteristic of the presence of chelating (**1**) and bischelating (**2**) bpm, as previously noted in parent bpm-containing copper(II) complexes.[9,10]

Physical Techniques. The IR spectra (KBr pellets) were recorded with a Perkin-Elmer 1750 FTIR spectrometer. Magnetic susceptibility measurements (2.0−300 K) under an applied field of 1 T were carried out with a Metronique Ingenierie MS03 SQUID magnetometer. It was calibrated with $(NH_4)_2Mn(SO_4)_2\cdot 6H_2O$. The corrections for the diamagnetism were estimated from Pascal constants as -207×10^{-6} (**1**) and -313×10^{-6} (**2**) cm^3 mol^{-1}.

X-ray Data Collection and Structure Refinement. Crystals of the dimensions 0.30 × 0.28 × 0.26 mm (**1**) and 0.28 × 0.22 × 0.24 mm (**2**) were mounted on a Siemens R3m/V automatic four-circle diffractometer and used for data collection. Diffraction data were collected at room temperature by using graphite-monochromated Mo Kα radiation ($\lambda = 0.710\ 73$ Å) with the $\omega-2\theta$ scan method. The unit cell parameters were determined from least-squares refinement of the setting angles of 25 reflections in the 2θ range 15−30°. Information concerning crystallographic data collections and structure refinements is summarized in Table 1. Examination of two standard reflections, monitored after 98 reflections, showed no sign of crystal deterioration. Data were corrected for Lorentz and polarization effects. ψ-Scan absorption correction[11] was used for complex **2**, whereas data for complex **1** were corrected by using the XABS program.[12] The maximum and minimum transmission factors were 0.986 and 0.422 for **1** and 0.401 and 0.293 for **2**. Of the 3162 (**1**) and 2431 (**2**) measured reflections in the 2θ range 3−54° with index ranges $-10 \le h \le 10$, $0 \le k \le 22$, and $0 \le l \le 11$ (**1**), $0 < h < 8$, $0 \le k \le 15$, and $-15 \le l \le 15$ (**2**), 2907 (**1**) and 2078 (**2**) were unique. From these, 2243 (**1**) and 1690 (**2**) were observed [$I > 3\sigma(I)$] and used for the refinement of the structures.

Table 2. Final Atomic Fractional Coordinates[a] and Equivalent Isotropic Displacement Parameters[b] for Non-Hydrogen Atoms of Compound **1**

atom	x/a	y/b	z/c	10^3U_{eq}/Å^2
Fe(1)	0.1176(1)	0.1848(1)	0.4274(1)	28(1)
Cl(1)	0.0149(1)	0.0703(1)	0.3287(1)	42(1)
Cl(2)	−0.1194(1)	0.2454(1)	0.4150(1)	41(1)
Cl(3)	0.1701(1)	0.2308(1)	0.2083(1)	49(1)
O(1)	0.2391(3)	0.2780(1)	0.5516(3)	41(1)
N(1)	0.3540(3)	0.1321(1)	0.5063(3)	32(1)
C(1)	0.4712(4)	0.1313(2)	0.4290(4)	41(1)
C(2)	0.6144(4)	0.0954(2)	0.4895(5)	47(1)
C(3)	0.6296(4)	0.0607(2)	0.6279(5)	47(1)
N(2)	0.5139(3)	0.0607(2)	0.7080(3)	40(1)
C(4)	0.3819(3)	0.0965(2)	0.6426(3)	30(1)
C(5)	0.2497(3)	0.1001(2)	0.7269(3)	28(1)
N(4)	0.2691(3)	0.0660(2)	0.8620(3)	38(1)
C(6)	0.1529(5)	0.0765(2)	0.9384(4)	46(1)
C(7)	0.0199(4)	0.1189(2)	0.8818(4)	43(1)
C(8)	0.0073(4)	0.1498(2)	0.7385(4)	35(1)
N(3)	0.1224(3)	0.1401(1)	0.6590(3)	28(1)
O(2)	0.0882(4)	0.4070(2)	0.5861(4)	78(1)

[a] Estimated standard deviations in the last significant digits are given in parentheses. [b] U values for anisotropically refined atoms are given in the form of the isotropic equivalent thermal parameter $U_{eq} = {}^1/_3(U_{11} + U_{22} + U_{33})$.

The structures were solved by standard Patterson methods and subsequently completed by Fourier recycling. All non-hydrogen atoms were refined anisotropically. The hydrogen atoms of the water molecules were located on a ΔF map and refined with constraints. The hydrogen atoms of bpm were set in calculated positions and refined as riding atoms with a common fixed isotropic thermal parameter. Full-matrix least-squares refinements were carried out by minimizing the function $\sum w(|F_o| - |F_c|)^2$ with $w = 1.000/[\sigma^2(F_o) + 0.0005(F_o)^2]$ (**1** and **2**). Models reached convergence with values of the R and R_w indices listed in Table 1. Criteria for satisfactory complete analysis were ratios of the root-mean-square shift to standard deviation being less than 0.005. The residual maxima and minima in the final Fourier-difference maps were 0.65 and −0.44 e Å^{-3} for **1** and 0.35 and −0.30 e Å^{-3} for **2**. The values of the goodness-of-fit are 1.45 (**1**) and 1.17 (**2**). Solutions and refinements were performed with the SHELXTL-PLUS system.[12] The final geometrical calculations were carried out with the PARST program.[13] The graphical manipulations were performed using the XP utility of the SHELXTL-PLUS system. Final fractional coordinates for non-hydrogen atoms are listed in Tables 2 (**1**) and 3 (**2**), whereas the main interatomic bond distances and angles are given in Tables 4 (**1**) and 5 (**2**). A complete list of crystal data and structure refinement, anisotropic temperature factors, hydrogen atom coordinates, nonessential bond distances and angles, least-squares planes, and intermolecular hydrogen bonds (Tables S1−S9) are available as Supporting Information.

Results and Discussion

Description of the Structures. $[Fe(bpm)Cl_3(H_2O)]\cdot H_2O$ (1). The structure of compound **1** consists of neutral $[Fe(bpm)Cl_3(H_2O)]$ mononuclear entities and water molecules of crystal-

(8) Nakamoto, K. *Infrared and Raman Spectra of Inorganic and Coordination Compounds*, 4th ed.; Wiley: New York, 1986; p 228.
(9) Castro, I.; Julve, M.; De Munno, G.; Bruno, G.; Real J.; Lloret, F.; Faus, J. *J. Chem. Soc., Dalton Trans.* **1992**, 1739.
(10) Julve, M.; Verdaguer, M.; De Munno, G.; Real, J. A.; Bruno, G. *Inorg. Chem.* **1993**, *32*, 795.
(11) North, A. C. T.; Philips, D. C.; Mathews, F. S. *Acta Crystallogr., Sect. A* **1968**, *24*, 351.
(12) SHELXTL-PLUS, Version 4.11/V Siemens Analytical X-Ray Instruments Inc., Madison, WI, 1990.
(13) Nardelli, M. *Comput. Chem.* **1983**, *7*, 95.

Table 3. Final Atomic Fractional Coordinates[a] and Equivalent Isotropic Displacement Parameters[b] for Non-Hydrogen Atoms of Compound **2**

atom	*x*/*a*	*y*/*b*	*z*/*c*	10^3U_{eq}/Å^2
Fe(1)	0.1777(1)	0.2162(1)	0.0803(1)	27(1)
Cl(1)	0.3825(1)	0.3540(1)	−0.0134(1)	44(1)
Cl(2)	0.1587(1)	0.3008(1)	0.2440(1)	39(1)
Cl(3)	0.4849(1)	0.1199(1)	0.1205(1)	45(1)
O(1)	−0.1222(3)	0.2745(2)	0.0290(2)	43(1)
N(1)	0.0081(3)	0.0655(2)	0.1316(2)	25(1)
C(1)	−0.0513(4)	0.0421(2)	0.2319(2)	29(1)
C(2)	−0.1462(4)	−0.0573(2)	0.2542(2)	33(1)
C(3)	−0.1820(4)	−0.1323(2)	0.1709(2)	32(1)
N(2)	−0.1252(3)	−0.1097(2)	0.0690(2)	27(1)
C(4)	−0.0330(3)	−0.0125(2)	0.0553(2)	24(1)
O(2)	−0.1470(5)	0.4328(2)	−0.1198(2)	68(1)

[a] Estimated standard deviations in the last significant digits are given in parentheses. [b] *U* values for anisotropically refined atoms are given in the form of the isotropic equivalent thermal parameter $U_{eq} = {}^1/_3(U_{11} + U_{22} + U_{33})$.

Table 4. Selected Bond Distances (Å) and Interbond Angles (deg)[a] for Compound **1**

Fe(1)−Cl(1)	2.305(1)	Fe(1)−Cl(2)	2.282(1)
Fe(1)−Cl(3)	2.252(1)	Fe(1)−O(1)	2.130(2)
Fe(1)−N(1)	2.209(3)	Fe(1)−N(3)	2.205(3)
Cl(1)−Fe(1)−Cl(2)	97.4(1)	Cl(1)−Fe(1)−Cl(3)	96.7(1)
Cl(2)−Fe(1)−Cl(3)	97.5(1)	Cl(1)−Fe(1)−O(1)	169.2(1)
Cl(2)−Fe(1)−O(1)	89.7(1)	Cl(3)−Fe(1)−O(1)	90.4(1)
Cl(1)−Fe(1)−N(1)	90.1(1)	Cl(2)−Fe(1)−N(1)	164.5(1)
Cl(3)−Fe(1)−N(1)	95.0(1)	O(1)−Fe(1)−N(1)	81.1(1)
Cl(1)−Fe(1)−N(3)	88.5(1)	Cl(2)−Fe(1)−N(3)	92.9(1)
Cl(3)−Fe(1)−N(3)	167.6(1)	O(1)−Fe(1)−N(3)	83.1(1)
N(1)−Fe(1)−N(3)	73.7(1)		

Hydrogen Bonds[b]

A	D	H	A···D	A···H−D
O(2)	O(1)	H(2w)	2.67(1)	173(3)
Cl(2a)	O(1)	H(1w)	3.24(1)	167(3)
N(4b)	O(2)	H(4w)	3.10(1)	177(3)

[a] Estimated standard deviations in the last significant digits are given in parentheses. [b] Symmetry code: (a) 0.5 + *x*, 0.5 − *y*, 0.5 + *z*; (b) −0.5 + *x*, 0.5 − *y*, −0.5 + *z*.

Table 5. Selected Bond Distances (Å) and Interbond Angles (deg)[a] for Compound **2**

Fe(1)−Cl(1)	2.269(1)	Fe(1)−Cl(2)	2.266(1)
Fe(1)−Cl(3)	2.311(1)	Fe(1)−O(1)	2.106(2)
Fe(1)−N(1)	2.223(2)	Fe(1)−N(2a)	2.244(2)
Cl(1)−Fe(1)−Cl(2)	100.1(1)	Cl(1)−Fe(1)−Cl(3)	94.9(1)
Cl(2)−Fe(1)−Cl(3)	97.5(1)	Cl(1)−Fe(1)−O(1)	91.1(1)
Cl(2)−Fe(1)−O(1)	90.8(1)	Cl(3)−Fe(1)−O(1)	168.7(1)
Cl(1)−Fe(1)−N(1)	166.0(1)	Cl(2)−Fe(1)−N(1)	93.2(1)
Cl(3)−Fe(1)−N(1)	87.7(1)	O(1)−Fe(1)−N(1)	84.2(1)
Cl(1)−Fe(1)−N(2a)	92.6(1)	Cl(2)−Fe(1)−N(2a)	165.5(1)
Cl(3)−Fe(1)−N(2a)	88.3(1)	O(1)−Fe(1)−N(2a)	81.9(1)
N(1)−Fe(1)−N(2a)	73.7(1)		

Hydrogen Bonds[b]

A	D	H	A···D	A···H−D
O(2)	O(1)	H(1w)	2.63(1)	172(3)
Cl(3b)	O(1)	H(2w)	3.40(1)	152(2)
Cl(1c)	O(2)	H(3w)	3.29(1)	146(2)
Cl(3d)	O(2)	H(4w)	3.42(1)	151(2)

[a] Estimated standard deviations in the last significant digits are given in parentheses. [b] Symmetry codes: (a) -*x*, −*y*, −*z*; (b) *x* − 1, *y*, *z*; (c) −*x*, 1 − *y*, −*z*; (d) −0.5 + *x*, 0.5 − *y*, −0.5 + *z*.

lization. These monomeric units form a chain through hydrogen bonds involving the coordinated water molecule (O(1)) and one of the coordinated chlorine atoms (Cl(2)) (see end of Table 4).

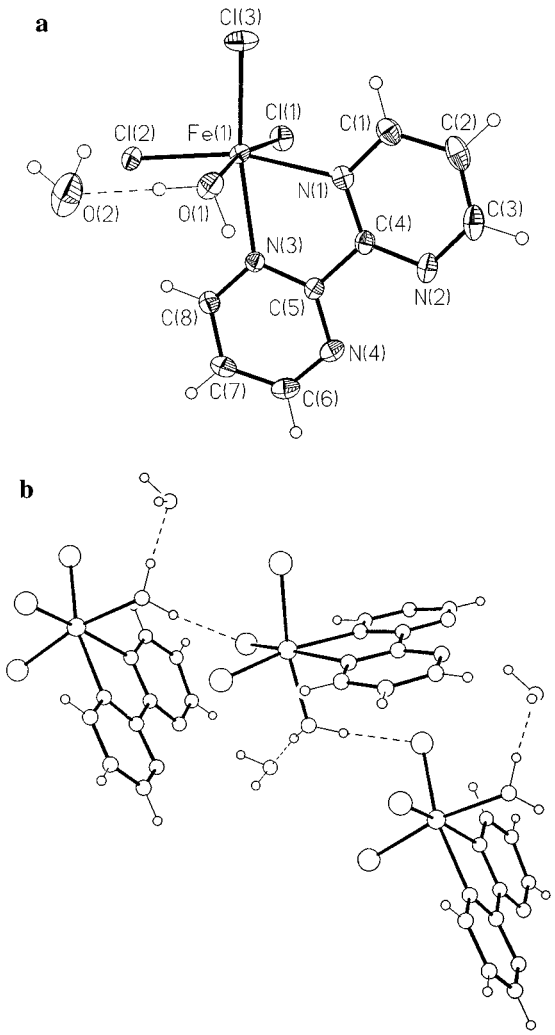

Figure 1. (a) Perspective drawing of complex **1** showing the atom numbering (the thermal ellipsoids are drawn at the 30% probability level). (b) Perspective drawing showing the chain arrangement in **1** caused by the hydrogen bonding (hydrogen bonds are represented by broken lines).

Neighboring chains are well separated from each other and are joined by van der Waals contacts. Perspective drawings of complex **1** showing the atom numbering in the monomeric unit and the resulting chain through hydrogen bonds are depicted in Figure 1, parts a and b, respectively.

Each metal atom is in a distorted octahedral environment with two chloride and two nitrogen atoms from bpm occupying the equatorial positions and a third chloride atom and a water molecule filling the axial ones. The Fe−N(bpm) bond distances in **1** [average value is 2.207(3) Å] are very close to that found in the mononuclear high-spin iron(II) complex $[Fe(py)_2(bpm)(NCS)_2]\cdot 0.25py$ (py = pyridine) [average value for the Fe−N(bpm) distance is 2.218(8) Å],[14] despite the higher oxidation degree of the metal ion in **1**. The $Fe-Cl_{eq}$ bond distances [average value is 2.267(1) Å] are somewhat shorter than the corresponding $Fe-Cl_{ax}$ [2.305(1) Å for Fe(1)−Cl(1)], but they are in agreement with that reported for other six-coordinated chloroiron(III) species.[15−18] The Fe−O bond length [2.130(2) Å for Fe(1)−O(1)] lies within the range of the Fe−O(water) bond distances in other aquairon(III) complexes from the

(14) Claude, R.; Real, J. A.; Zarembowitch, J.; Kahn, O.; Ouahab, L.; Grandjean, D.; Boukheddaden, K.; Varret, F.; Dworkin, A. *Inorg. Chem.* **1990**, *29*, 4442.

literature [values ranging from 1.98 to 2.18 Å].[15−21] The main distortion from the octahedral environment of the metal atom in **1** is due to the reduced value of the bite angle of the bpm ligand [73.7(1)° for N(1)−Fe(1)−N(3)]. The best equatorial plane is defined by the N(1), N(3), Cl(2), and Cl(3) atoms [largest deviation from the mean plane is 0.043(3) Å for N(1)]. The iron atom is 0.138(1) Å out of this plane.

The chelating bpm in **1** is clearly distorted due to its coordination; it has a bite distance N(1)···N(3) of 2.646(4) Å, while the N(2)···N(4) distance is 2.750(4) Å. The pyrimidyl rings of the bpm group are planar, as expected, with deviations not greater than 0.020(3) Å from the mean planes. The bpm ligand as a whole is almost planar [the dihedral angles between the pyrimidine rings are 6.2(1)°]. The carbon−carbon and carbon−nitrogen bond lengths agree with those observed in other metal complexes with chelating bpm.[4,9,10,14,22] The carbon−carbon inter-ring bond length [1.492(5) Å for C(4)−C(5)] is practically the same as that found in free bpm in the solid state.[23] The shortest intrachain metal−metal distance is 5.957(2) Å [Fe(1)···Fe(1a), Fe(1)···Fe(1b), (a) = 0.5 + *x*, 0.5 + *y*, 0.5 + *z*; (b) = −0.5 + *x*, 0.5 − *y*, −0.5 + *z*], whereas the shortest metal−metal separation between neighboring chains is 7.038(1) Å.

$[Fe_2(bpm)Cl_6(H_2O)_2]\cdot 2H_2O$ (2). The structure of compound **2** consists of centrosymmetric $[Fe_2(bpm)Cl_6(H_2O)_2]$ dinuclear entities (Figure 2a) and water molecules of crystallization which are held together through an extensive network of hydrogen bonds (see end of Table 5). The two metal atoms within the dinuclear unit are connected by a tetradentate bpm group with an inversion center located at the center of the carbon−carbon bond of the two pyrimidyl rings. The dinuclear units are held together by means of H-bonds in which Cl(3) (axial) atoms and coordinated water molecules are involved, propagating as a ladder-like chain along the *x* axis. Other H-bonds, occurring by means of coordinated and uncoordinated water molecules and Cl(1) (equatorial) or Cl(3) (axial) atoms, link the chains in the *xy* (Figure 2b) or *yz* plane to yield a three-dimensional network.

Complex **2** can be considered to result from **1** through coordination of its two nitrogen-bpm terminal atoms to a hypothetical $[FeCl_3(H_2O)]$ unit. As in **1**, the environment of each metal atom is octahedrally elongated, the N atoms occupying the equatorial plane. The Fe−Cl_{eq} bond distances [average 2.267(1) Å] are somewhat shorter than the Fe−Cl_{ax} [2.311(1) Å for Fe(1)−Cl(3)]. The iron to water oxygen bond distance is a bit shorter than in **1** [2.106(2) Å for Fe(1)−O(1)], whereas the Fe−N bonds average 2.239(2) Å, a value which is significantly longer than that found in **1**. This last structural feature is most likely due to the different coordination mode

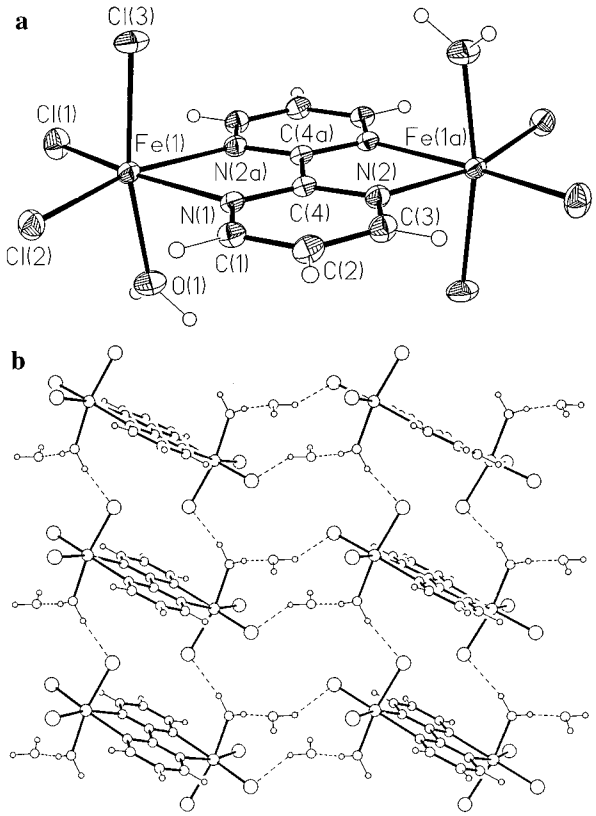

Figure 2. (a) Perspective drawing of complex **2** showing the atom numbering (the thermal ellipsoids are drawn at the 30% probability level). (b) Perspective view of **2** along the *z* axis illustrating the hydrogen-bonded sheetlike network (hydrogen bonds are represented by broken lines).

adopted by bpm in these complexes (chelating in **1** and bischelating in **2**). The value of the angle subtended by bpm at the metal atom is identical to that observed in **1**. The best equatorial plane is defined by the N(1), N(2a), Cl(1), and Cl(2) atoms [largest deviation from the mean plane is 0.043(2) Å for N(2a)]. The iron atom is 0.099(1) Å out of this plane.

The pyrimidyl rings are planar, as expected, with deviations not greater than 0.006(3) Å from the mean planes. The bpm ligand as a whole is planar, and the metal atom is displaced by 0.088(1) Å from this plane toward Cl(3). The bite distance of bischelating bpm [N(1)···N(2a) distance] is 2.679(3) Å. The dihedral angle between the equatorial plane and that of bpm amounts to only 2.0(1)°. The carbon−carbon inter-ring bond length in **2** [1.482(5) Å for C(4)−C(4a)] is a bit shorter than that observed in **1**. The intramolecular metal−metal separation across bpm is 5.952(1) Å [Fe(1)···Fe(1a), (a) = −*x*, −*y*, *z*], a value which is very close to that reported for parent bpm-bridged iron(II) complexes.[24] The shortest intermolecular metal−metal distance is 6.422(2) Å [Fe(1)···Fe(1b), Fe(1)···Fe(1c), (b) = −1 + *x*, *y*, *z*; (c) = 1 + *x*, *y*, *z*].

Magnetic Properties. The magnetic behavior of complexes **1** and **2** is shown in Figures 3 and 4 as the χ_M versus *T* plot, χ_M being the molar magnetic susceptibility and *T* the temperature. Both curves are characteristic of an antiferromagnetic interaction between single-ion sextuplet states: the value of χ_M at 290 K

(15) Ferrari, A.; Cavalca, L.; Tani, M. E. *Gazz. Chim. Ital.* **1957**, *87*, 22.
(16) Lind, M. D. *J. Chem. Phys.* **1967**, *47*, 990.
(17) Szymanski, J. T. *Acta Crystallogr.* **1979**, *B35*, 1958.
(18) Greedan, J. E.; Hewitt, D. C.; Faggiani, R. F.; Brown, I. D. *Acta Crystallogr.* **1980**, *B36*, 1927.
(19) Hair, N. J.; Beattie, J. K. *Inorg. Chem.* **1977**, *16*, 245 and references.
(20) Hazell, A.; Jensen, K. B.; McKenzie, C. J.; Toflund, H. *J. Chem. Soc., Dalton Trans.* **1993**, 3249.
(21) Wikinson, E. C.; Dong, Y.; Que, L., Jr. *J. Am. Chem. Soc.* **1994**, *116*, 8394.
(22) (a) Castro, I.; Sletten, J.; Glærum, L. K.; Lloret, F.; Faus, J.; Julve, M. *J. Chem. Soc., Dalton Trans.* **1994**, 2777. (b) Castro, I.; Sletten, J.; Glærum, L. K.; Cano, J.; Lloret, F.; Faus, J.; Julve, M. *J. Chem. Soc., Dalton Trans.* **1995**, 3207. (c) De Munno, G.; Julve, M.; Real J. A. *Inorg. Chim. Acta* **1997**, *255*, 185. (d) De Munno, G.; Viau, G.; Julve, M.; Lloret, F.; Faus, J. *Inorg. Chim. Acta* **1997**, *257*, 121.
(23) Fernholt, L.; Rømming D.; Sandal, S. *Acta Chem. Scand., Ser. A* **1981**, *35*, 707.
(24) (a) Real, J. A.; Zarembowitch, J.; Kahn, O.; Solans, X. *Inorg. Chem.* **1987**, *26*, 6, 2939. (b) Andrés, E.; De Munno, G.; Julve, M.; Real, J. A.; Lloret, F. *J. Chem. Soc., Dalton Trans.* **1993**, 2169. (c) De Munno, G.; Julve, M.; Real, J. A.; Lloret, F.; Scopelliti, R. *Inorg. Chim. Acta* **1996**, *250*, 81.

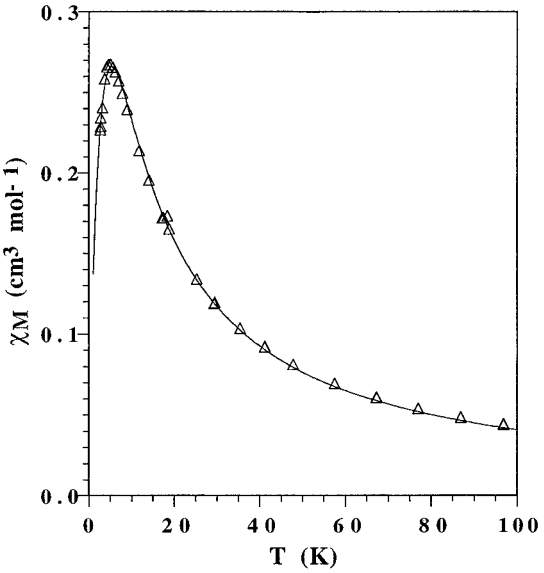

Figure 3. Thermal dependence of molar magnetic susceptibility for complex **1**: (△) experimental data; (–) best theoretical fit (see text).

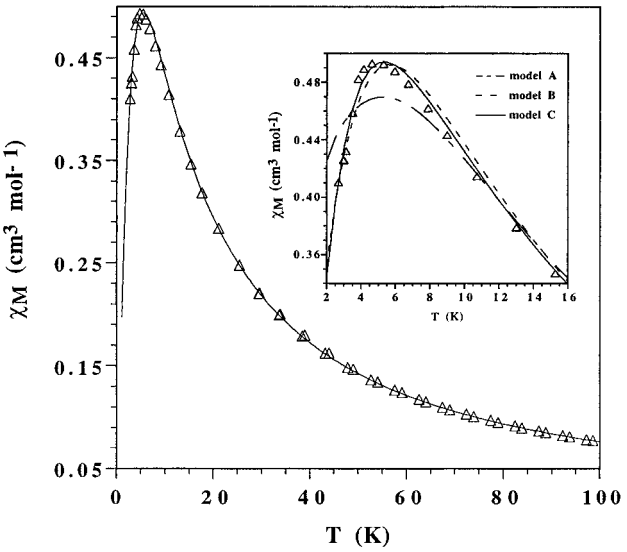

Figure 4. Thermal dependence of molar magnetic susceptibility for complex **2**: (△) experimental data; (–) best theoretical fit through model C (see text). The insert shows the quality of the fit through models A−C in the vicinity of the maximum.

is in the range expected for one (**1**) and two (**2**) S = $^5/_2$ states [$\chi_M T$ = 4.24 (**1**) and 8.53 (**2**) cm^3 mol^{-1} K versus the calculated values of 4.33 and 8.66 cm^3 mol^{-1} K for one and two noninteracting high-spin Fe(III) ions, respectively], increases as the temperature is lowered and until a maximum is reached [T_{max} = 5.0 (**1**) and 5.2 (**2**) K], and finally decreases.

With the uniform chain structure of compound **1** being taken into account (see Figure 1b), its magnetic susceptibility data were analyzed by using Fisher's nearest-neighbor classical Heisenberg coupling model for infinite linear chains[25] through eq 1

$$\chi_M = \frac{35N\beta^2g^2}{12kT}\frac{1+u(K)}{1-u(K)} \quad (1)$$

where

$$u(K) = \coth K - (1/K) \quad (2)$$

and

$$K = 35J/4kT \quad (3)$$

which has been derived from the Hamiltonian given in eq 4

$$\hat{H} = -J\sum_{i=1}^{n}\hat{S}_1\cdot\hat{S}_{i+1} - g\beta\sum_{i=1}^{n}H\cdot\hat{S}_i \quad (4)$$

with $S_i = S_{i+1} = {}^5/_2$. The parameters N, β, g, and k have their usual meanings. Least-squares analysis of the susceptibility data lead to $J = -0.68$ cm^{-1}, $g = 1.99$, and $R = 1.9 \times 10^{-4}$. R is the agreement factor defined as $\sum_i[(\chi_M)_{obs}(i) - (\chi_M)_{calc}(i)]^2/\sum_i[(\chi_M)_{obs}(i)]^2$. The theoretical curve matches very well the experimental data, as shown in Figure 3. Two main points deserve to be outlined in the magnetostructural study of complex **1**: first, the crucial role of structural knowledge in the analysis of the magnetic properties of a given compound and, second, the relevance of the hydrogen bonds in mediating electronic interactions between paramagnetic centers. In the present case, the monomeric [Fe(bpm)Cl$_3$(H$_2$O)] units are linked through hydrogen bonds involving the coordinated water molecule (O(1)) and one of the equatorial chlorine atoms (Cl(2)) (see Figure 1b), yielding a uniform chain arrangement with intrachain metal−metal separation of 5.957(2) Å. This hydrogen-bonding pattern [O(1)−H(1w)···Cl(2a), the distance between O(1) and Cl(2a) being 3.24(1) Å] accounts for the significant antiferromagnetic coupling observed in **1** ($J = -0.68$ cm^{-1}). Keeping in mind the great distance between the interacting iron(III) ions and the presence of five unpaired electrons on each metal site, the magnitude of the magnetic coupling in **1** is relatively large. In the course of our current research work, we have had the occasion to check the efficiency of hydrogen bonding in transmitting exchange coupling, the most appealing result being the giant antiferromagnetic coupling between copper(II) ions through the bihydroxide anion.[26]

The structure of complex **2** shows the occurrence of bis-chelating bpm in contrast to complex **1**, where this ligand adopts the chelating mode. The resulting [Fe$_2$(bpm)Cl$_6$(H$_2$O)$_2$] dinuclear units are linked through hydrogen bonds involving the coordinated water molecule and the axially coordinated chlorine atom [O(1)−H(2w)···Cl(3b)] to yield a ladder-like chain along the x axis (see Figure 2b). This hydrogen-bonding pattern resembles that of complex **1**, the separation between the acceptor (chlorine) and the donor (oxygen) atoms being somewhat greater in **2** [3.40(1) Å in **2** versus 3.24(1) Å in **1**]. These ladder-like chains are connected through hydrogen bonds involving the coordinated and crystallization water molecules and the chlorine atoms along both the y (Figure 2b) and z axes to yield a three-dimensional network. In light of the magnetostructural data of complex **1** and the well-known efficiency of bridging bpm to transmit antiferromagnetic interactions when acting as bridging ligand,[10,22a,b,27] the only relevant exchange pathways in complex **2** occur within the ladder-like chain. It seems clear that the

(25) Fisher, M. E. *Am. J. Phys.* **1964**, *32*, 343.

(26) De Munno, G.; Viterbo, D.; Caneschi, A.; Lloret, F.; Julve, M. *Inorg. Chem.* **1994**, *33*, 1585.

(27) (a) Julve, M.; De Munno, G.; Bruno, G.; Verdaguer, M. *Inorg. Chem.* **1988**, *27*, 7, 3160. (b) De Munno, G.; Real, J. A.; Julve, M.; Muñoz, M. C. *Inorg. Chim. Acta* **1993**, *211*, 227. (c) De Munno, G.; Julve, M.; Lloret, F.; Cano, J.; Caneschi, A. *Inorg. Chem.* **1995**, *34*, 2048.

(28) (a) Hong, D. M.; Wei, H. H.; Gan, L. L.; Lee, G. H.; Wang, Y. *Polyhedron* **1996**, *15*, 2335. (b) De Munno, G.; Poerio, T.; Julve, M.; Lloret, F.; Viau, G.; Caneschi, A. *J. Chem. Soc., Dalton Trans.* **1997**, 601.

Table 6. Selected Magnetostructural Data for **2** and Bpm-Bridged Mn(II) and Fe(II) Complexes

metal ion	compd	M−N(bpm)[a]/Å	$d_{M\cdots M}$[b]/Å	$-J$[c]/cm^{-1}	ref
Mn(II)	$[Mn_2(bpm)(H_2O)_4(SO_4)_2]$	2.31	6.123(2)	1.1	6
	$[Mn(bpm)(NO_3)_2]$	2.36	6.239(1) 6.247(1)	0.93	28
	$[Mn(bpm)(NCO)_2]$	2.35	6.234(1)	1.1	28b
	$[Mn_2(bpm)_3(NCS)_4]$	2.36	6.223(1)	1.19	22d
	$[Mn_2(bpm)_3(NCSe)_4]$	2.35	6.211(1)	1.20	22d
Fe(III)	**2**	2.23	5.952(1)	1.1	this work
Fe(II)	$[Fe_2(bpm)_3(NCS)_4]$	2.27	6.050	4.1	24a
	$[Fe_2(bpm)(H_2O)_8](SO_4)_2\cdot 2H_2O$	2.22	5.836(1)	3.4	24b
	$[Fe_2(bpm)(H_2O)_6(SO_4)_2]$	2.22	5.909(1)	3.1	24b
	$[Fe(bpm)(NCS)_2]$	2.24	5.960(1)	3.5	24c

[a] Average value for the metal-to-nitrogen (bridging bpm) bond. [b] Metal−metal separation across bpm. [c] Exchange interaction through bridging bpm.

exchange interaction between iron(III) ions from adjacent ladder-like chains [transmitted through coordinated chlorine and uncoordinated and coordinated water] can be neglected against that mediated by a water molecule and a chlorine atom within the ladder-like chain. Accordingly, the most appropriate model to treat the magnetic susceptibility data of complex **2** would be a classical spin ladder-like chain with two exchange coupling parameters, one through bridging bpm (J) and the other through the chlorine−water hydrogen bond (J'). Unfortunately, no analytical expression has been proposed for this case.

In order to analyze the magnetic behavior of **2** and to check our hypothesis (magnetic ladder-like behavior), we have used three models denoted A, B, and C. In model A, the magnetic susceptibility data of complex **2** were analyzed in terms of an isotropic exchange interaction for a magnetically isolated bpm-bridged iron(III) dimer ($\hat{H} = -J\hat{S}_1\cdot\hat{S}_2$ with $S_1 = S_2 = {}^5/_2$) through

$$\chi_M = \frac{2N\beta^2 g^2}{kT}\frac{x + 5x^3 + 14x^6 + 30x^{10} + 55x^{15}}{1 + 3x + 5x^3 + 7x^6 + 9x^{10} + 11x^{15}} \quad (5)$$

with

$$x = \exp(J/kT) \quad (6)$$

The least-squares fit leads to $J = -1.27$ cm^{-1}, $g = 1.92$, and $R = 1.4 \times 10^{-3}$. In model B, interdimer interactions are considered, and consequently, T in eq 5 is replaced by $T - \theta$ where $\theta = zJ'S(S + 1)/3k$ (θ accounting for the magnetic interaction between the bpm-bridged dimers). The results of the fit are $J = -0.87$ cm^{-1}, $g = 1.88$, $zJ' = -0.37$ cm^{-1}, and $R = 3.4 \times 10^{-4}$. Finally, in model C we have treated the susceptibility data of complex **2** as in **1** (classical spin chain through hydrogen bonding) but introducing a zJ' parameter accounting for the interaction through bridging bpm. The best-fit parameters for this approach are $J = -0.44$ cm^{-1}, $g = 1.93$, $zJ' = -0.74$ cm^{-1}, and $R = 1.0 \times 10^{-4}$. The results of the fit through models A−C are shown in Figure 4. As can be seen on this figure, the fits are not very good and the computed g value remains too low. Model A provides the worst fit in the vicinity of the susceptibility maximum (see inset of Figure 4) and clearly points out that the exchange interaction through hydrogen bonding cannot be discarded. Models B and C agree in the fact that the antiferromagnetic couplings though bridging bpm and hydrogen bonding should be very close. The fit through model C is the best, and both the antiferromagnetic coupling through hydrogen bonding (-0.44 cm^{-1}) and that through bridging bpm ($J' = -0.74$ cm^{-1} with $z = 1$) are as expected. An antiferromagnetic coupling of -0.68 cm^{-1} has been found for **1**, so the somewhat weaker antiferromagnetic coupling in **2** (-0.44 cm^{-1}) seems reasonable because of the lengthening of the coordinated water to chlorine atom distance [3.40(1) Å in **2** versus 3.24(1) Å in **1**]. As far as the value of the antiferromagnetic coupling through bridging bpm is concerned (-0.74 cm^{-1}), it is close to those reported for bpm-bridged Mn(II) compounds where the interacting local spins have the same size ($S = {}^5/_2$), as shown in Table 6. Pertinent magnetostructural data concerning bpm-bridged iron(II) complexes are included in this table aiming at illustrating the influence of the oxidation state of a given metal ion on the magnitude of the exchange coupling, everything else being equal. So, a comparison between the Fe(II) family ($S = 2$) and complex **2** ($S = {}^5/_2$) shows that the larger antiferromagnetic coupling in the lower oxidation state compounds cannot be attributed to structural factors: the metal−metal separation across bpm is practically identical. The removal of one electron when going from Fe(II) to Fe(III) causes a decrease of the energy of the 3d magnetic orbitals and, consequently, diminishes the energy gap between them and the symmetry-adapted HOMOs of the bpm. This would lead to a better overlap between them, and a stronger antiferromagnetic coupling is to be expected for the Fe(III) compound. The opposite trend occurs. Most likely, the greater diffusivity of 3d orbitals of the Fe(II) versus that of Fe(III) becomes the leading factor and accounts for the observed trend.

To conclude, the main aspects of the present work can be summarized as follows: (i) the preparation of mono- and dinuclear bpm-containing iron(III) complexes which can be used as precursors of higher nuclearity systems has been achieved for the first time; (ii) the structural knowledge is crucial when investigating the magnetic behavior (case of complexes **1** and **2**), and hydrogen bonding can play a determinant role in the magnetic coupling as shown for complex **1**; (iii) although the accurate determination of the magnetic coupling through bpm in **2** requires the use of an appropriate ladder-like model, the rough value that we have obtained reveals that bpm is able to transmit a significant antiferromagnetic coupling between Fe(III) ions separated by more than 5.9 Å.

Acknowledgment. Financial support from the Spanish DGICYT through Project PB94-1002 and the Italian Ministero dell'Università e della Ricerca Scientifica e Tecnologica is gratefully acknowledged. Thanks are due to Dr. A. Caneschi from the Università degli Studi di Firenze (Italy) for the magnetic measurements of complexes **1** and **2**. G.V. is indebted to the Ministerio Español de Educación y Ciencia for a postdoctoral grant.

Supporting Information Available: Tables of crystal data and structure refinement (Table S1), anisotropic thermal parameters for non-hydrogen atoms (Tables S2 and S3), hydrogen-atom coordinates (Tables S4 and S5), nonessential bond distances and angles (Tables S6 and S7), and least-squares planes (Tables S8 and S9) (12 pages). Ordering information is given on any current masthead page.

IC971110I